Journal of Glaciology

Article

Cite this article: Falcini FAM, Krabbendam M, Selby KA, Rippin DM (2021). Using bed-roughness signatures to characterise glacial landform assemblages beneath palaeo-ice sheets. *Journal of Glaciology* 1–15. https://doi.org/10.1017/jog.2021.122

Received: 15 March 2021
Revised: 25 October 2021
Accepted: 26 October 2021

Keywords:
Drumlins; glacial geomorphology; remote sensing

Author for correspondence:
Francesca A. M. Falcini,
E-mail: f.a.falcini@gmail.com

cambridge.org/jog

Using bed-roughness signatures to characterise glacial landform assemblages beneath palaeo-ice sheets

Francesca A. M. Falcini[1], Maarten Krabbendam[2], Katherine A. Selby[1] and David M. Rippin[1]

[1]Department of Environment and Geography, Wentworth Way, University of York, York, UK and [2]British Geological Survey, The Lyell Centre, Research Avenue South, Edinburgh, UK

Abstract

Palaeo-glacial landforms can give insights into bed roughness that currently cannot be captured underneath contemporary-ice streams. A few studies have measured bed roughness of palaeo-ice streams but the bed roughness of specific landform assemblages has not been assessed. If glacial landform assemblages have a characteristic bed-roughness signature, this could potentially be used to constrain where certain landform assemblages exist underneath contemporary-ice sheets. To test this, bed roughness was calculated along 5 m × 5 m resolution transects (NEXTMap DTM, 5 m resolution), which were placed over glacial landform assemblages (e.g. drumlins) in the UK. We find that a combination of total roughness and anisotropy of roughness can be used to define characteristic roughness signatures of glacial landform assemblages. The results show that different window sizes are required to determine the characteristic roughness for a wide range of landform types and to produce bed-roughness signatures of these. Mega scale glacial lineations on average have the lowest bed-roughness values and are the most anisotropic landform assemblage.

Introduction

Glacial landform assemblages left behind by Pleistocene ice sheets of North America and Northern Europe provide information on palaeo ice-sheet dynamics (Stokes and Clark, 1999; Stokes, 2018). Certain ice–bed conditions and processes can be derived from landform assemblages and compared to those operating in present-day ice sheets (e.g. landform elongation ratios and ice velocity; Kleman and others, 1997; Stokes and Clark, 2001; Stokes, 2018). Landform assemblages can also be used to reconstruct palaeo-ice sheets (e.g. Hughes and others, 2014) and as analogues for current ice-sheet beds (Evans and others, 1999; Clark and others, 2012; Bradwell and Stoker, 2015). An advantage of studying palaeo-ice sheets is that their former beds are visible and can be analysed with high-resolution digital elevation models (DEMs; e.g. Dowling and others, 2015; Margold and others, 2015). In contrast, access to the bed of present-day ice sheets is restricted (Fretwell and others, 2013), and relies on sparse boreholes and remote-sensing methods such as seismic surveys and radio-echo sounding (RES). Such data are commonly of low resolution and are acquired in widely spaced (≥500 m) flight lines (e.g. Bingham and others, 2007; Rippin and others, 2014; King and others, 2016). This means that over large parts of present-day ice sheets there are uncertainties on sediment cover (Kulessa and others, 2017), thermal state (MacGregor and others, 2016), bed-elevation (Fretwell and others, 2013) and bed-roughness (Bingham and Siegert, 2009; Falcini and others, 2018; Cooper and others, 2019). Although many definitions of bed roughness exist (Smith, 2014), we define subglacial bed-roughness in this paper as the vertical variation of terrain over a given horizontal distance (Rippin and others, 2014). The roughness of subglacial topography, especially at shorter length-scales, affects drag at the ice– interface and is a primary control on basal sliding speeds, alongside effective water pressure and basal ice temperature (Schoof, 2002; Siegert and others, 2005; Rippin, 2013). Uncertainties in bed-roughness measurements and in how ice flows over obstacles means that roughness in general is not taken into account in ice-sheet modelling, despite its probable importance (Bingham and others, 2017; Nias and others, 2016; Leong and Horgan, 2020).

Many previous studies have measured bed-roughness for both contemporary (RES data) and palaeo-ice-stream (DEMs) beds at scales that were too large (transect spacing of 30–50 km, along-transect resolution of 1.85 km–75 m and window sizes of 320 m–70 km) to capture glacial landforms (Siegert and others, 2004; Rippin and others, 2006; Bingham and others, 2007; Rippin and others, 2014; Lindbäck and Pettersson, 2015). Yet, an increasing number of studies have demonstrated that small-scale glacial landforms exist underneath contemporary-ice sheets (e.g. King and others, 2007, 2009; Jezek and others, 2011; Bingham and others, 2017). These high-resolution (e.g. ≤500 × ≤500 m line spacing and ≤7.5 m along track spacing) studies, however, only cover small areas of contemporary-ice-stream beds, providing an incomplete analysis of landform location and distribution. It has not been feasible to expand these high-resolution studies across an entire contemporary-ice sheet due to the technical, cost and time constraints (see methods in King and others, 2016). Recent study by

Holschuh and others (2020) suggests future studies will be able to map larger areas at high resolution using airborne radar.

Palaeo-ice-sheet beds commonly have a complex and diverse range of landforms from drumlins to mega scale glacial lineations (MSGLs) (Stokes and Clark, 2001; Krabbendam and others, 2016; Clark and others, 2018b). Palaeo-ice-sheet beds provide an opportunity to measure bed roughness not just at the ice-stream scale (e.g. Gudlaugsson and others, 2013; Lindbäck and Pettersson, 2015; Falcini and others, 2018) but also at the landform scale. Yet, why should we measure bed roughness of glacial landform assemblages? If certain types of glacial landform assemblages have a range of bed-roughness values that are characteristic to them (bed-roughness signature), such information could be used to infer where landforms occur underneath contemporary-ice sheets (Stokes, 2018). This would improve our understanding of contemporary-ice-sheet beds, for example, by providing information on landform types, sediment cover vs hard-beds, sliding velocity (e.g. King and others, 2007), whether landforms are in a steady state (Hillier and others, 2013) or represent previous ice dynamics, and could also improve palaeo-ice-sheet models.

In this study, we investigate whether certain glacial landforms assemblages have characteristic bed-roughness signatures. We choose four study areas, all in the UK, each with a uniform glacial landform assemblage i.e. only one type of landform. These include cnoc and lochan, drumlins, megagrooves, and MSGLs. We also choose two areas that have mixed glacial landforms. The bed roughness of all six areas is quantified along sections parallel and orthogonal to palaeo-ice flow (1-D), and bed-roughness anisotropy is calculated from these 1-D results. Additionally, bed roughness is quantified using a 2-D method. We test whether uniform glacial landform assemblages have characteristic bed-roughness signatures i.e. can be differentiated from areas of mixed glacial landform assemblages, using both bed roughness and anisotropy of bed-roughness measurements.

Study areas and data

The British and Irish ice sheet (BIIS) was located on the edge of the Eurasian ice sheet complex (Hughes and others, 2014), and was active during the Devensian 116–11.5 ka BP (Clark and others, 2012). The Last Glacial Maximum (LGM) for the BIIS occurred between 30 and 21 ka BP, with retreat and readvance during 19–17 ka BP (Chiverrell and Thomas, 2010), followed by final deglaciation around 14–13 ka BP (Clark and others, 2012). Evidence from ice-rafted debris (e.g. Peck and others, 2006), numerical modelling (e.g. Hubbard and others, 2009) and ice flow set patterns (e.g. Hughes and others, 2014), indicates that the BIIS was often unstable, with pronounced and repeated ice advances and retreats. Adjustments to these instabilities left behind landforms that have a complicated formation history as shown by cross cutting or overprinting features (Livingstone and others, 2008, 2010; Davies and others, 2019). Over 170 000 landforms have been mapped from the BIIS (Clark and others, 2018a), including areas, which are categorised as 'classic' glacial landform assemblages e.g. drumlin swarms.

The high-resolution NEXTMap Digital Terrain Model (DTM) was used to extract elevation data required for bed-roughness calculations. The NEXTMap DTM has a 5 m horizontal resolution and a 1 m vertical resolution (Bradwell, 2013). The DTM tiles were downloaded from the Centre for Environmental Data Analysis (CEDA) Archive (Intermap Technologies, 2009). Landform distribution was assessed using BRITICE version 2.0 (Clark and others, 2018a).

Study areas were chosen within the UK that had classic examples of uniform (one type) landforms i.e. cnoc and lochan, drumlins, megagrooves and MSGLs (areas 1–4, Figs 1c–f, Table 1). Individual landforms had to be large enough to be visible on NEXTMap DTM (>5 m wide and long, and >1 m high), so landforms at the meso- (1 m–1 km) and macro-scale (1 km–100 km) categories (Bennett and Glasser, 2009) were selected. For areas of uniform landforms, our selection criteria required that the landforms have a single palaeo-ice-flow direction and no (or few) other landforms occurred in the study area. In addition, two areas were chosen that had a mix of different landforms, one in an upland and one in a lowland setting, to test whether uniform and mixed areas of glacial landforms can be differentiated from each other (areas 5 and 6, Figs 1g–h, Table 1).

Methods

In glaciology, bed-roughness is often calculated using fast Fourier transform analysis (FFT; e.g. Taylor and others, 2004; Li and others, 2010; Spagnolo and others, 2017) or using standard deviation (SD; e.g. Rippin and others, 2014; Cooper and others, 2019). These methods provide a statistical analysis of the vertical variation of elevation along a transect (Cooper and others, 2019). Both FFT analysis and SD produce similar spatial distributions of bed-roughness values (Rippin and others, 2014; Falcini and others, 2018). An advantage of SD is that bed-roughness values are calculated in units of distance i.e. metres, (Cooper and others, 2019) and it requires fewer data processing steps. We chose the SD method to quantify bed roughness in 1-D and 2-D. The 1-D approach measures bed roughness along transects – both parallel and orthogonal to the palaeo-ice flow – that sample the NEXTMap DTM. The 2-D approach measures bed roughness within a moving window (with a specific area and shape) centred at every pixel of the data domain. We used both approaches to assess which provided the clearest bed-roughness signatures.

1-D method for determining roughness

The 1-D method analyses along-transect elevation variations and thus imitates the data used to calculate bed roughness underneath contemporary ice streams as derived from RES surveys (i.e. grids of transects) (e.g. Siegert and others, 2004; Bingham and others, 2007; Falcini and others, 2018). Transect grids with 5 m × 5 m spacing were created (ArcMap, 'Create Fishnet' tool) and rotated so that the transects were aligned approximately parallel and orthogonal to palaeo-ice flow (Fig. 2). The orientation of transects relative to ice flow has a clear effect on bed-roughness calculations: transects parallel to ice flow commonly give considerably lower roughness values than transects orthogonal to ice flow (Bingham and others, 2017; Falcini and others, 2018; Cooper and others, 2019). This can be attributed to ice flow streamlining of the bed; a clear link with fast ice-surface velocity and smooth beds parallel but not orthogonal to flow was found by Cooper and others (2019). Ice-flow direction was interpreted from landform orientations (Stokes and Clark, 1999). Ice-flow direction is not necessarily in a straight line over a given distance. For example, ice flow is curved at areas 2 and 4 (Figs 1d, f). At area 4 the ice-flow curvature was overcome as the study area was easily split, but it was not possible in area 2. Area 6 also has complicated flow directions: during the LGM flow direction was approximately east to west, but in the Younger Dryas a plateau ice cap formed and ice flow was strongly topographically constrained with variable ice-flow directions (Finlayson and others, 2011). The transects were positioned approximately east to west to match the dominant flow direction of the last BIIS because this larger ice mass likely had more impact on the roughness values.

Points were added along the transects at 5 m intervals (QGIS, 'QChainage' plugin) to match the resolution of the NEXTMap DTM (Fig. 2). Areas that crossed lakes (OS Meridian 2 Lake shapefile) were removed to reduce a smoothing bias in the

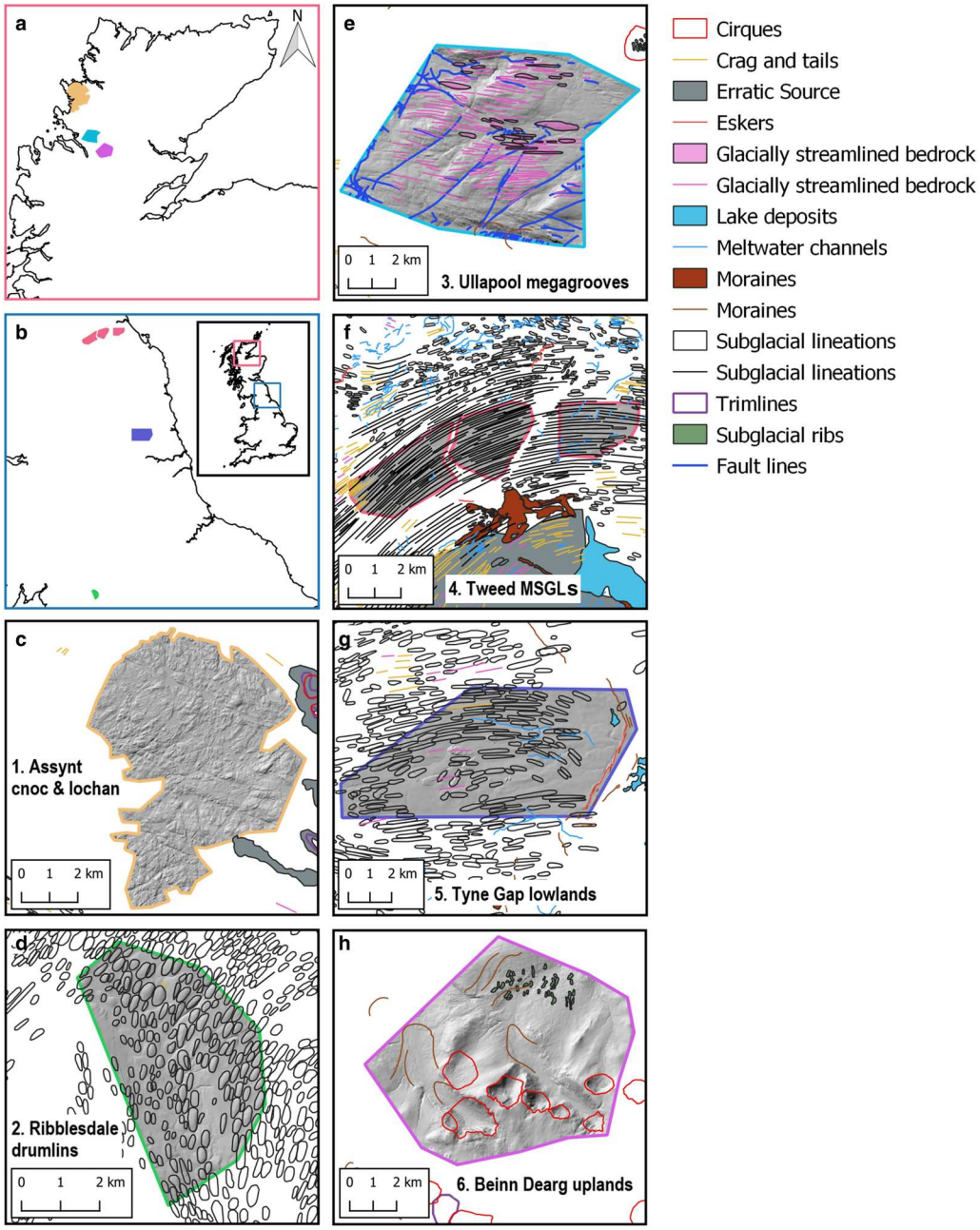

Fig. 1. (a), (b) Location of study areas (inset map in b). (a) Location of (c), (e), (h), while (b) shows (d), (f), (g). Each area is shown with NEXTmap DTM (Intermap Technologies, 2009) overlain by Britice glacial landforms (Clark and others, 2018a). (c) Site 1: Assynt. Palaeo-ice flow was ≈ east to west. (d) Site 2: Ribblesdale. Palaeo-ice flow was ≈ northeast to southwest. (e) Site 3: Ullapool. Palaeo-ice flow was ≈ east to west. (f) Site 4: Tweed. Palaeo-ice flow was ≈ west to east. (g) Site 5: Tyne Gap. Palaeo-ice flow was ≈ west to east. (h) Site 6: Beinn Dearg. Palaeo-ice flow was ≈ east to west.

bed-roughness calculations (Gudlaugsson and others, 2013; Falcini and others, 2018). The NEXTMap DTM pixel values (elevation) were extracted and added to the grid point shapefiles, which were then split into individual transects. This enables bed roughness to be calculated separately for parallel and orthogonal to ice-flow transects.

Roughness is strongly scale dependent: a region of 'flat' terrain can be rough on the small scale, whereas a high-relief landscape can be smooth on the large scale (Shepard and Campbell, 1999; Prescott, 2013). Due to the size variation of landforms, moving windows of 100 m and 1 km were chosen to capture bed-roughness signatures at a range of scales (Table 1). Before bed-roughness was calculated, the data were detrended (Fig. 2) to remove large wavelengths caused by mountains and valleys, which would otherwise dominate the bed-roughness values (Shepard and others, 2001; Smith, 2014). The data were detrended by calculating the mean for each point along a transect within a moving window (100 m and 1 km) and subtracted from the original to leave the detrended output. SD of elevation was then calculated along every transect using the same moving window sizes that were used for detrending. The transects were then combined and converted to a raster for easier display.

Anisotropy (directionality) calculation

Anisotropy (also referred to as directionality; Rippin and others, 2014) is a useful metric for interpreting bed-roughness measurements as it quantifies the difference between roughness parallel ($R_{\parallel}$) and roughness orthogonal ($R_{\perp}$) to ice flow (Smith, 2014). Anisotropy can only be calculated at points where parallel and orthogonal transects cross, which is why we created 1-D transects from 2-D raster DTMs. Using the transect grids created in section

Table 1. Area information

Number	Name	Description	Category	Grid reference	Reference
1	Assynt	Macroscale landscape of glacial erosion	Cnoc & Lochan	204274, 913979 : 219789, 933882	Rea and Evans (1996); Krabbendam and Bradwell (2014)
2	Ribblesdale	Mesoscale depositional landforms 95–530 m long 55–355 m wide 1 – 4:1 elongation	Drumlins	377075, 473454 : 381886, 480210	Mitchell (1994); Clark and others (2009)
3	Ullapool	Macroscale erosional landforms 1–2 km long 50–120 m wide 10–20 m deep 6 – 25:1 elongation	Megagrooves	213786, 894499 : 226444, 903043	Bradwell (2005); Bradwell and others (2008); Krabbendam and others (2016)
4	Tweed	Macroscale depositional landforms 2–16.5 km long 8 – 23:1 elongation	MSGLs	371008, 637141 : 398551, 648095	Clapperton (1971); Clark (1993); Everest and others (2005); Hughes and others (2010)
5	Tyne Gap	Lowland area with a mixture of erosional & depositional landforms	Lowlands	402867, 575447 : 416518, 583336	Livingstone and others (2010, 2012); Krabbendam and Glasser (2011)
6	Beinn Dearg	Upland area with a mixture of erosional & depositional landforms	Uplands	222916, 884827 : 234426, 894578	Finlayson and Bradwell (2007); Finlayson and others (2011))

Descriptions include size and elongation ratios of the landforms where available from the literature.

'1-D method for determining roughness', the anisotropy ratio (Ω) was calculated using the following equation from Smith and others (2006):

$$\Omega = \frac{R_{\parallel} - R_{\perp}}{R_{\parallel} + R_{\perp}} \quad (1)$$

where when $R_{\parallel}$ is the roughness of a transect parallel to ice flow and $R_{\perp}$ is the roughness orthogonal to ice flow. Anisotropy Ω is closer to 1 when $R_{\parallel}$ is higher than $R_{\perp}$, is 0 when bed roughness is isotropic, and closer to -1 when $R_{\perp}$ is higher than $R_{\parallel}$. Note that anisotropy Ω is zero both on a perfect smooth plane, but also in a very rough, but truly random landscape.

2-D method

The 2-D method uses the NEXTMap DTM data in raster format i.e. no transects were created. The NEXTMap DTM (elevation data) was clipped to the extent of all the study areas (Fig. 2). The clipped raster was then detrended by calculating mean elevation rasters (ArcMap, 'Focal Statistics' tool) and then subtracting these from the original DTM. Similar to the 1-D method, window sizes of 100 m and 1 km were used to capture roughness at two scales. SD of elevation was calculated for the detrended rasters using a moving window (same size as used for detrending, 100 m and 1 km).

Cluster analysis

To further test whether bed roughness and anisotropy data from the areas fall into landform groups, cluster analysis was carried out. Cluster analysis places data into groups (the number of groups is specified by the user). This is done by placing each individual data point into a group that has the nearest centroid (multidimensional equivalent of the mean; Crawley, 2007). We used the partitioning based *K*-means cluster analysis function in R, which uses the algorithm developed by Hartigan and Wong (1979). The variables used were bed-roughness (mean values calculated from the parallel and orthogonal transect crossover locations) and anisotropy across individual areas. For each window size, cluster analysis was calculated for areas 1–4 and 6, and then just for areas 1–4 to establish if the uniform landform types could be grouped more easily without the mixed area. Area 5 was not included due to striping in the anisotropy data (see 'Striping error' section). The bed roughness and anisotropy data used were from the interquartile range. Statistics on how well the cluster analysis performed when compared to the landform groupings were calculated using the confusion Matrix function in R, and are reported in the figure captions.

Results

Area 1: Assynt cnoc and lochan landscape

The cnoc and lochan landscape of Assynt in NW Scotland (Fig. 1) is a macroscale landscape of glacial erosion, characterised by abundantly exposed bedrock with numerous hills (cnocs), lakes (lochan) and small valleys. The landscape is typical for glacially eroded basement or 'shield' terrain (Rea and Evans, 1996; Krabbendam and Bradwell, 2014).

The cnoc and lochan landscape is somewhat rougher orthogonal to palaeo-ice-flow direction rather than parallel to it (Figs 3a–d). The cnoc and lochan has low anisotropy values, with a mean of −0.1 for the 1 km window values and 0 for the 100 m window values (Table 2). The roughest locations (red areas) calculated using a 1 km window (Figs 3a, c, g) are not picked up when using a 100 m window (Figs 3b, d, h). These areas are located over bedrock highs with steep slopes. The roughest locations (red areas) calculated using a 100 m window are located at lake edges and existing faults lines (Figs 3b, d, h).

Area 2: Ribblesdale drumlins

The Ribblesdale drumlins of the Yorkshire Dales (Fig. 1) have been described as 'classically shaped' because they are half egg-shaped features, which appear as blisters superimposed on the landscape (Clark and others, 2009; Spagnolo and others, 2012). Drumlins are sediment and/or rock formed, smooth, oval-shaped hills and are categorised as mesoscale landforms (Menzies, 1979; Benn and Evans, 2010). The drumlins in Ribblesdale have a length of 95–530 m, widths of 55–355 m and elongation ratios of 1–4 : 1 (Mitchell, 1994; Clark and others, 2009). Figures 3a–d

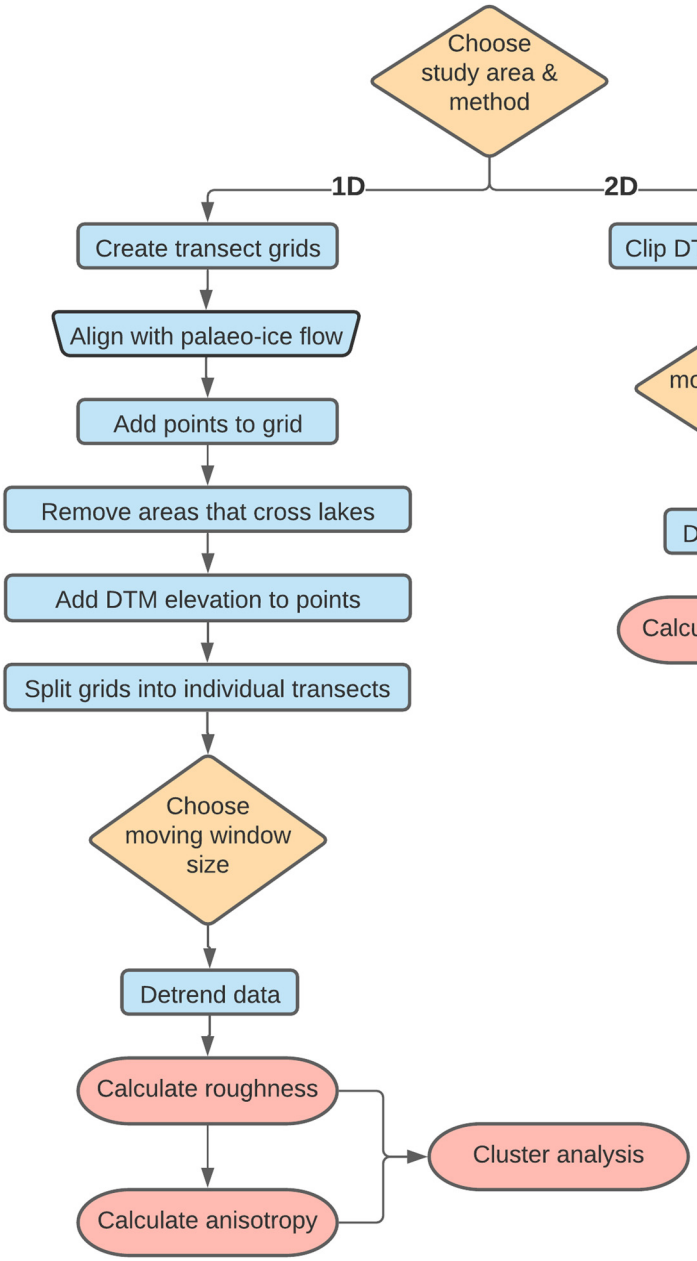

Fig. 2. Flow chart detailing the steps required to calculate bed roughness using both the 1-D and 2-D methods described in the 'Methods' section.

show that the drumlin field is rougher orthogonal rather than parallel to the palaeo-ice-flow direction. The same spatial pattern is shown by the anisotropy values, with higher roughness values orthogonal to palaeo-ice flow (Figs 4e–f) and mean anisotropy values of −0.1 and −0.2 (Table 2). The roughest values are located over small post-glacial streams (Figs 4a—d, h), and thus arguably not relevant for the overall analysis. Individual drumlins can be seen more clearly using the 100 m window size, and have high bed-roughness values on the drumlin sides but not on the crests (Figs 4d, h). It should be noted that not all the drumlins are exactly aligned to the transects due to the slight curving of the ice-flow direction.

Area 3: Ullapool megagrooves

The Ullapool megagrooves located in NW Scotland (Fig. 1) are erosional, macroscale landforms described as metre-scale deep grooves in rock, and are located in an area measuring 6 km by 10 km (Bradwell, 2005; Krabbendam and others, 2016; Newton and others, 2018). The megagrooves have a typical length of 1000–2000 m, width of 50–120 m, depth of 10–20 m and elongation ratios of 6–25 : 1 (Bradwell and others, 2008). The megagrooves are considerably rougher orthogonal to palaeo-ice-flow direction than parallel to the palaeo-ice-flow direction (Figs 5a–d). The anisotropy values support this observation (Figs 5e, f) with mean anisotropy between −0.2 and −0.4 (Table 2). Some pre-existing geological faults that are orientated diagonally across the megagrooves (Fig. 1e) can be seen in the parallel to palaeo-ice-flow and 2-D data (Figs 5a, b, h). Roughness along the transects orthogonal to ice flow is greater for deeper megagrooves (up to 6 m) than for shallower ones (up to 3 m).

Area 4: Tweed MSGLs

The Tweed MSGL landsystem located in NE England (Fig. 1) comprises MSGLs: depositional, macroscale landforms formed at the base of the Tweed Palaeo-Ice Stream (Everest and others, 2005). MSGLs are described as very elongated ridges, which are spaced parallel to each other (Clark, 1993; Spagnolo and others, 2014). The Tweed MSGLs are 2–16.5 km long and have elongation ratios of 8–23 : 1 (Everest and others, 2005; Hughes and others, 2010).

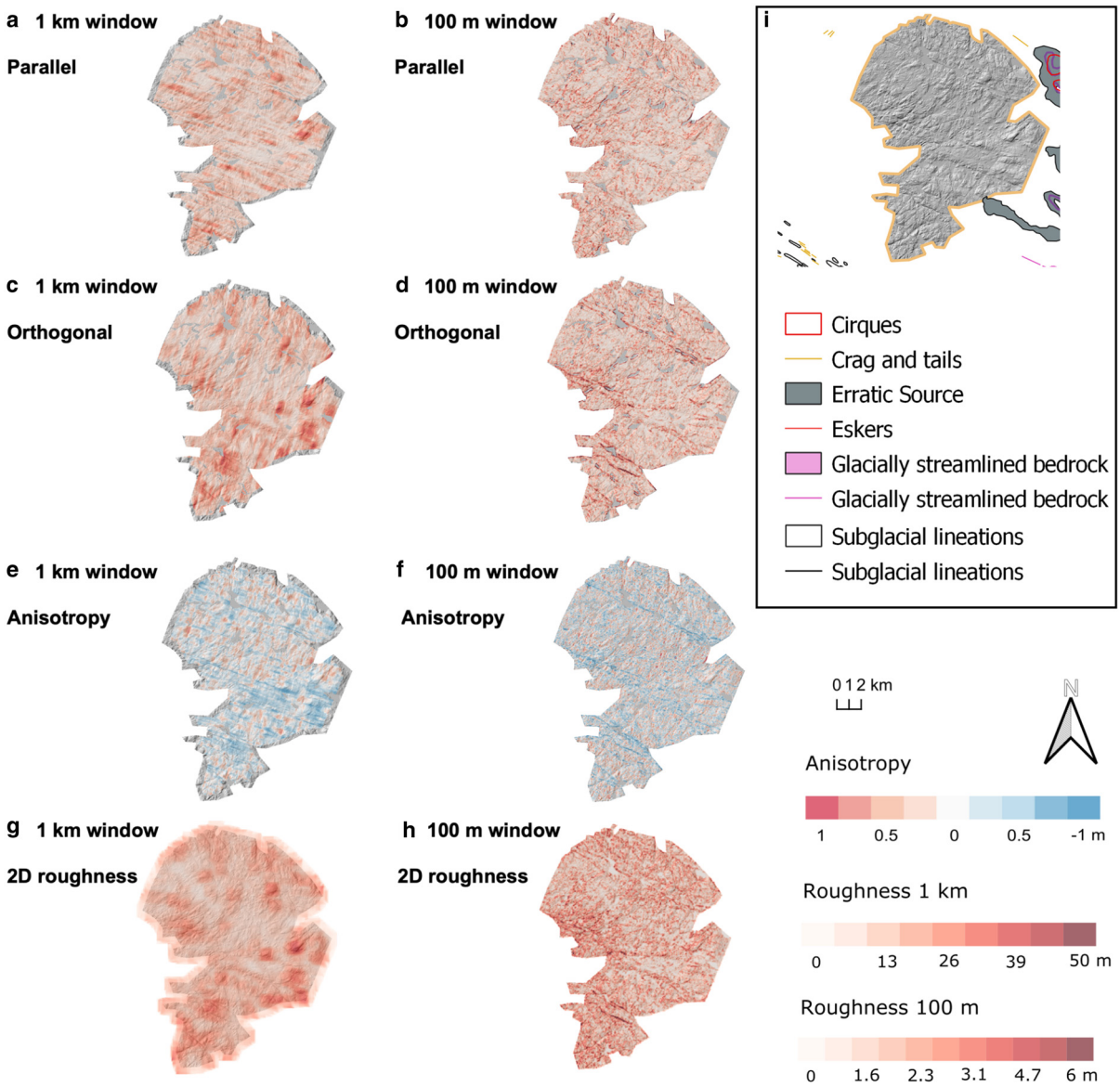

Fig. 3. Bed roughness over the Assynt cnoc and lochan (area 1). Bed roughness was calculated parallel (a, b) and orthogonal (c, d) to palaeo-ice flow direction (1-D), and for all flow directions (2-D; g, h), using SD with 1 km and 100 m window sizes. (e, f) Anisotropy of bed roughness was calculated at the crossover points between parallel and orthogonal transects for both window sizes. Between −1 and 0, orthogonal -roughness values dominate (blue). Between 0 and 1, parallel bed-roughness values dominate (red). At 0, bed roughness is isotropic (white). (i) Location area from Fig. 1 overlain with glacial landforms for comparison.

Table 2. Statistics of bed roughness and anisotropy for all areas (m)

Area	Window size	Roughness			Anisotropy		Cluster analysis	
		Mean	Range	IQR	Mean	IQR	All	Uniform
1. Assynt cnoc and lochan	1 km	12.9	42.6	5.6	−0.1	0.3	64	74
	100 m	1.2	74.9	0.9	0	0.5	97	71
2. Ribblesdale drumlins	1 km	6.2	12.7	2.2	−0.1	0.3	98	100
	100 m	0.6	6.9	0.4	−0.2	0.5	40	39
3. Ullapool megagrooves	1 km	10.2	41.8	6.2	−0.2	0.4	49	78
	100 m	1	39.7	0.7	−0.3	0.4	80	85
4. Tweed MSGLs	1 km	2.5	7.6	1.4	−0.4	0.39	100	100
	100 m	0.2	1.4	0.12	−0.2	0.43	96	97
4. Tweed MSGLs	1 km	2.5	7.6	1.4	−0.4	0.36		
(no striping)	100 m	0.2	1.4	0.12	−0.3	0.37		
5. Tyne Gap lowlands	1 km	2.4	13.2	1.39	−0.1	0.56		
	100 m	0.2	5.8	0.08	0	0.64		
6. Beinn Dearg uplands	1 km	16.6	91.7	15.98	0	0.5	62	
	100 m	0.8	27.9	0.6	0	0.5	77	

The statistics were calculated by combining values for both flow directions. Two sets of values were reported for the Tweed due to the striping in the anisotropy; one for the whole site, and one without the eastern section that has the striping. IQR = interquartile range. Accuracy of the cluster analysis is reported (%) for all sites analysed and where only the uniform landform assemblages were analysed (Figs 8 and 9).

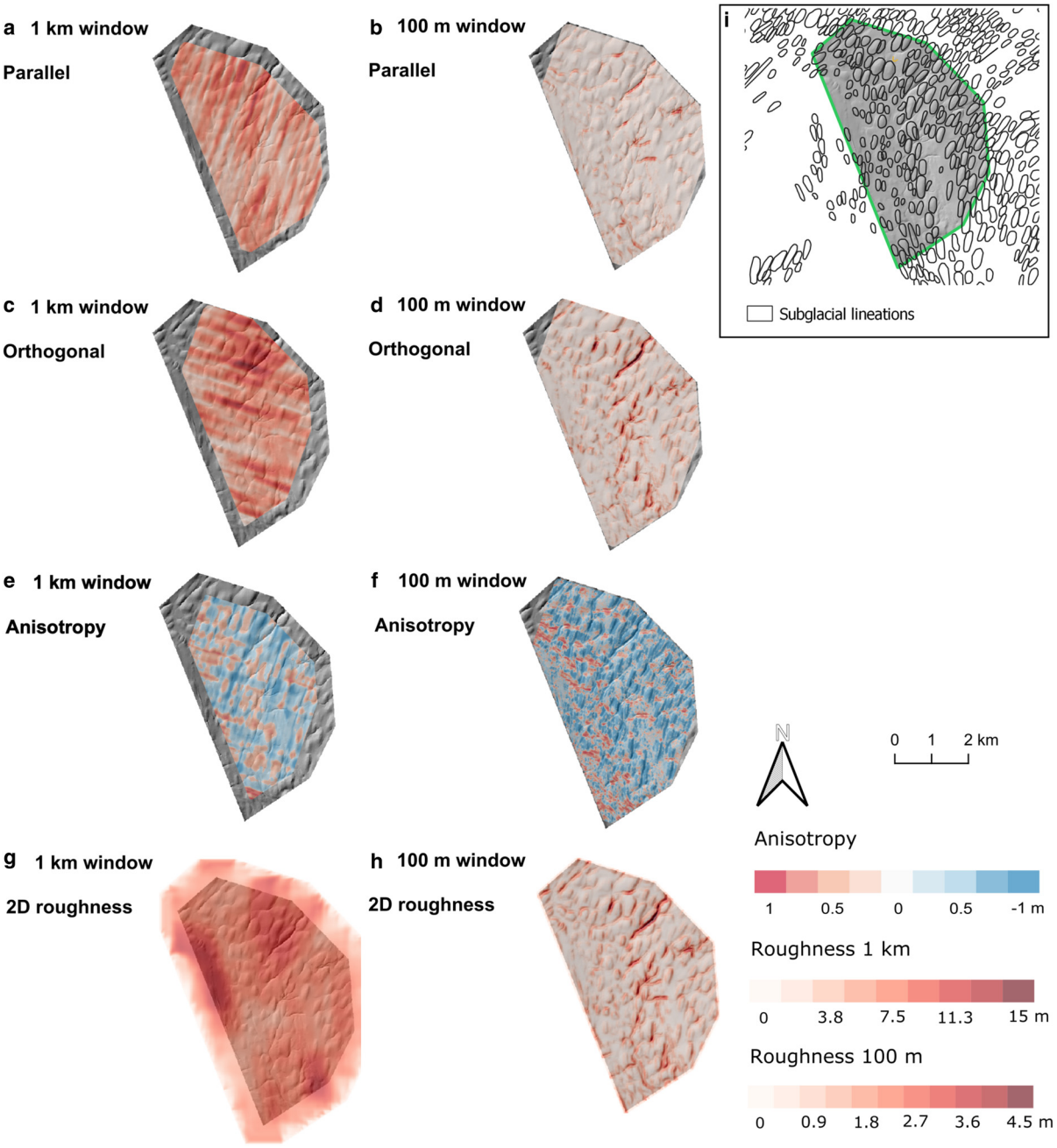

Fig. 4. Bed roughness over the Ribblesdale drumlins (area 2). Bed roughness was calculated parallel (a, b) and orthogonal (c, d) to palaeo-ice flow direction (1-D), and for all flow directions (2-D; g, h), using SD with 1 km and 100 m window sizes. (e, f) Anisotropy of bed roughness was calculated at the crossover points between parallel and orthogonal transects for both window sizes. Between −1 and 0, orthogonal bed-roughness values dominate (blue). Between 0 and 1, parallel bed-roughness values dominate (red). At 0, bed roughness is isotropic (white). (i) Location area from Fig. 1 overlain with glacial landforms for comparison.

Like the megagrooves and drumlins, the MSGLs in area 4 are rougher orthogonal rather than parallel to palaeo-ice-flow direction (Figs 6a–d). This is also shown by the anisotropy values (Figs 6e, f), with mean anisotropy values of −0.4 and −0.3 for the 1 km and 100 m windows, respectively (Table 2) being the highest of any area. Area 4 has the lowest mean roughness values compared to the other uniform landforms (areas 1–3; Table 2). The crests of the MSGLs are shown as rough by the parallel to palaeo-ice flow (for 1 km window size results; Fig. 6a), in contrast to drumlin crests.

Area 5: Tyne Gap lowlands

Located in NE England (Fig. 1), area 5 is part of the Tyne Gap Palaeo-Ice Stream (Livingstone and others, 2015), and is a lowland area that has a mix of depositional and erosional landforms (Krabbendam and Glasser, 2011). Elongation ratios vary from 1–10 : 1 (Livingstone and others, 2010, 2012).

The bed-roughness results from the glaciated lowland area suggest that it is slightly rougher orthogonal rather than parallel to palaeo-ice-flow direction (Figs 7a–d). This is shown by the low anisotropy result (Figs 7e–f) for the 1 km window only, which has a mean value of −0.1. The 100 m window has a mean value of 0 and is isotropic (Table 2). The bed-roughness values for area 5 are similar to those from area 4, and these areas are the smoothest overall (Table 2). The roughest area (in red) shown in the 1 km window results is an area of exposed bedrock (Figs 1g, 7a, c), which is also shown as rough (red) for the 100 m window results, as are some of the meltwater channels (Figs 1g, 6b, d). The esker and moraines that are located at the

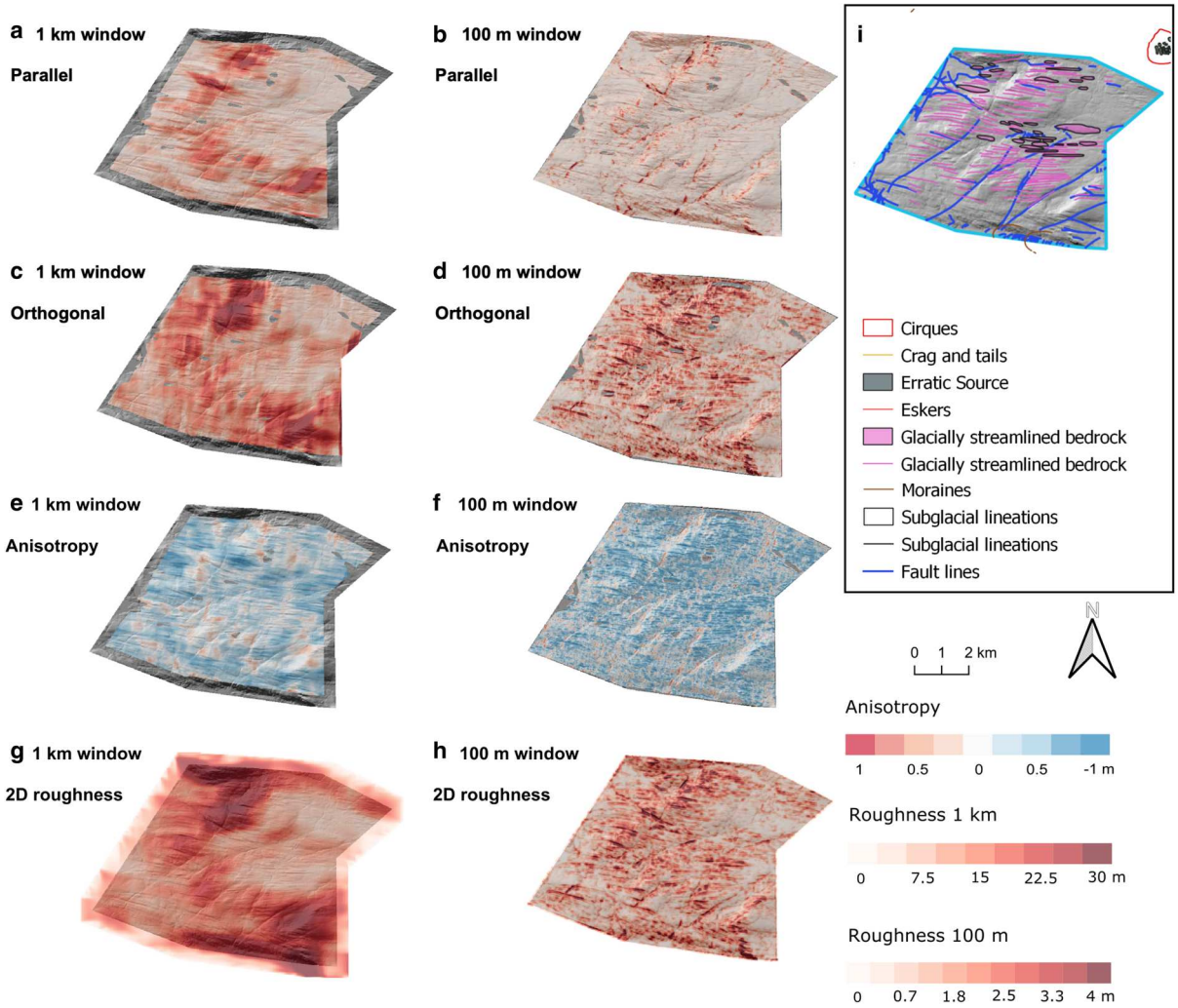

Fig. 5. Bed roughness over the Ullapool megagrooves (area 3). Bed roughness was calculated parallel (a, b) and orthogonal (c, d) to palaeo-ice flow direction (1-D), and for all flow directions (2-D; g, h), using SD with 1 km and 100 m window sizes. (e, f) Anisotropy of bed roughness was calculated at the crossover points between parallel and orthogonal transects for both window sizes. Between −1 and 0, orthogonal bed-roughness values dominate (blue). Between 0 and 1, parallel bed-roughness values dominate (red). At 0, bed roughness is isotropic (white). (i) Location area from Fig. 1 overlain with glacial landforms for comparison.

far east of area 5 (Fig. 1g) are picked out as rough by the 100 m window data (Figs 7b, d) and have >0 anisotropy values (Fig. 7f). The majority of the drumlins (Fig. 1g) are not shown as rough on the 100 m window data (Figs 7b, d, h). Those that are rough appear to be rock cored (Livingstone and others, 2008; Krabbendam and Glasser, 2011).

Area 6: Beinn Dearg uplands

Located in Beinn Dearg massif, NW Scotland, area 6 is an upland area that has a mix of depositional and erosional landforms (Fig. 1 Finlayson and others, 2011). This area comprises cirques and glacial valleys, as well as Rogen moraines (Hughes and others, 2010; Finlayson and others, 2011).

The mean anisotropy for both window sizes is 0 (Table 2), and there is no clear spatial pattern of anisotropy in relation to the glacial landforms (Figs 8e–f). The highest bed-roughness values (red) are found on the steep cirques (Figs 1h and 8a–d, g, h), which is expected. Both parallel and orthogonal to palaeo-ice flow results derived from a 100 m window size show the ribbed moraines as rougher than the surrounding areas (Figs 1h and 8b, d, h), but this is not shown by the 1 km window size results (Figs 8a, c, g) and cannot be seen in the anisotropy data (Figs 8e–f). In the 100 m window results, there are other features in close proximity to the rogen moraines that have similar roughness values and spatial patterns (Figs 8b, d). The origin of these features, which were not mapped by Clark and others (2018a) or Finlayson and others (2011), is not clear.

Comparison of results

A summary of all the bed roughness and anisotropy data across the areas can be seen in Table 2. The MSGLs (area 4) are the most anisotropic and least rough of all the landforms at the 1 km window size scale (Table 2). The mixed uplands (area 6) is the roughest area at the 1 km window scale and is the only one that is isotropic with the 1 km window size (Table 2). At this window size, the cnoc and lochan and megagrooves areas (3 and 1) have very similar mean bed roughness and anisotropy values (Table 2). Using the 100 m window size, the megagrooves and cnoc and lochan areas can be distinguished more clearly with a large difference in anisotropy (− 0.3 vs 0; Table 2). At this window size, both cnoc and lochan and uplands areas (1 and 6) are isotropic, while all the other areas have a negative anisotropy (Table 2). The results from the cluster analysis show that the MSGLs (area 4) can be clearly grouped for both the 1 km window and 100 m windows (Figs 9 and 10); the accuracy of the cluster analysis (how accurate it is at placing values from the MSGLs in

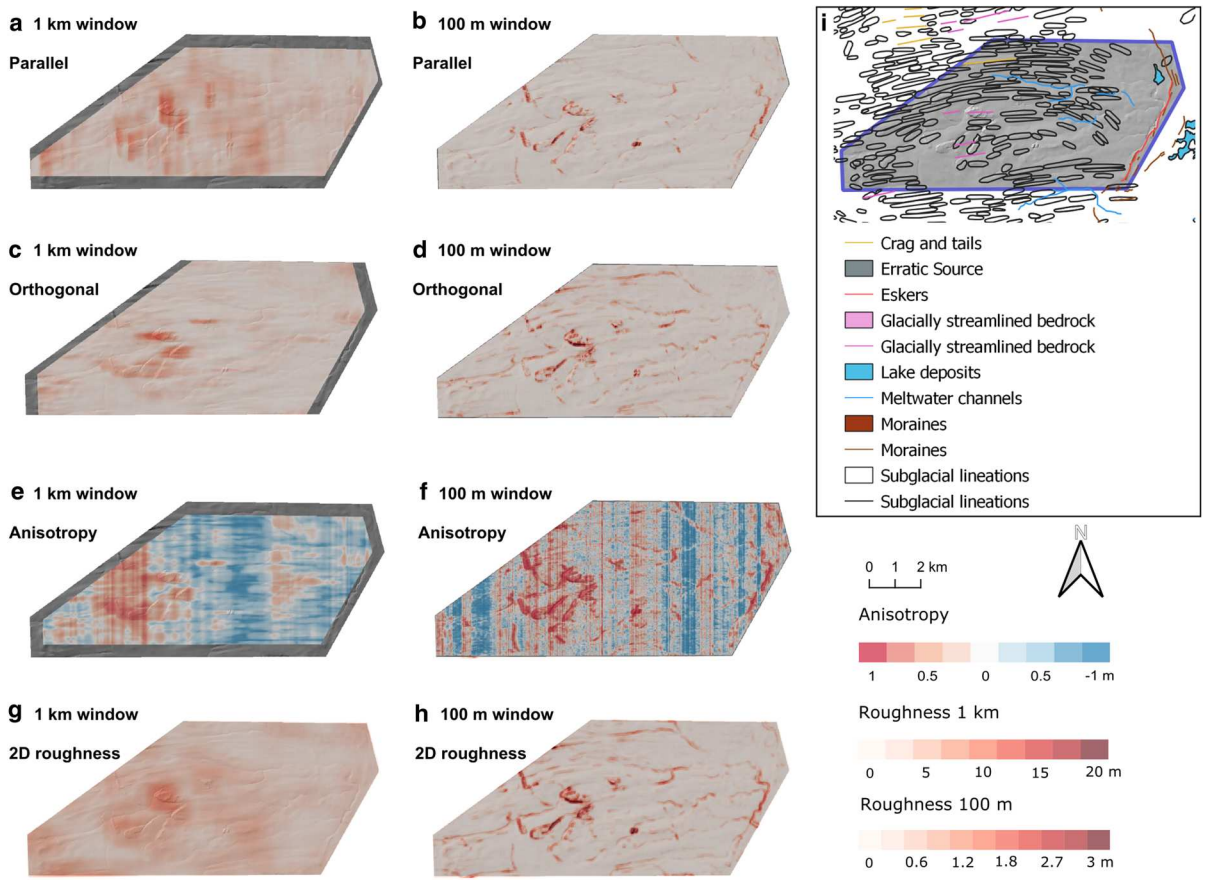

Fig. 6. Bed roughness over the Tweed MSGLs (area 4). Bed roughness was calculated parallel (a, b) and orthogonal (c, d) to palaeo-ice flow direction (1-D), and for all flow directions (2-D; g, h), using SD with 1 km and 100 m window sizes. (e, f) Anisotropy of bed roughness was calculated at the crossover points between parallel and orthogonal transects for both window sizes. Between −1 and 0, orthogonal bed-roughness values dominate (blue). Between 0 and 1, parallel bed-roughness values dominate (red). At 0, bed roughness is isotropic (white). (i) Location area from Fig. 1 overlain with glacial landforms for comparison.

the same cluster group) is 100 and 96% respectively. The cluster analysis also shows that the cnoc and lochan and megagrooves areas (1 and 3) are better separated for the 100 m window results compared to the 1 km window results (Figs 9b, d, 10b, d). The accuracy for the cnoc and lochan and megagrooves areas (1 and 3) when groups 1–4 and 6 were used in the cluster analysis was 64 and 49% respectively for the 1 km window data (Fig. 9b), and 67 and 80% respectively for the 100 m window data (Fig. 10b). When the upland area (6) was removed from the cluster analysis, the accuracies for the cnoc and lochan and megagrooves areas (1 and 3) was 74 and 78% respectively for the 1 km window data (Fig. 9d), and 71 and 85% respectively for the 100 m window data (Fig. 10d). The accuracy for placing values correctly in the megagroove (area 3) cluster group is much better for the 100 m window compared to the 1 km window, but this is not the case for the cnoc and lochan (area 1). For the drumlins (area 2), the cluster analysis showed clear results for the 1 km window data with accuracies of 98 and 100% (Fig. 9b). However, for the 100 m window data, the cluster analysis had accuracies of 40 and 39% as there was a lot of crossover with other cluster groups (Fig. 10b).

Striping error

Due to the striping in the anisotropy results for the eastern section of area 4 (MSGL; Figs 6e, f) and area 5 (lowlands; Figs 7e, f), these data were not included in Table 2 or the cluster analysis to ensure they did not bias the results. The striping might be caused by the orientation of the transects. For these areas only, the transects are aligned exactly north south and east west, which is the same as the DTM pixel orientation. The striping is much more prevalent in the 100 m window results compared to the 1 km window results (e.g. Figs 7e vs 7f). Striping artefacts by their nature are anisotropic, and have been shown to be scale-dependent, having a greater effect on DTM curvature distributions at smaller window sizes (Sofia and others, 2013). The collection of DTM data along lines can cause striping artefacts during interpolation that can impact roughness results (Sofia and others, 2013; Trevisani and Cavalli, 2016). NEXTMap DTM data were collected using parallel flight lines, with three orthogonal flight lines per 200 km × 200 km block to aid systematic error removal (Mercer, 2007). A visual inspection of the NEXTMap DTM shows that there is no striping at areas 4 and 5. Thus, this was an unexpected error, which was only visible in the anisotropy measurements. Transects should not be aligned with the DTM pixel direction to avoid this error.

Discussion

Roughness and anisotropy signal of landform assemblages

The results show that glacial landforms assemblages do have characteristic bed-roughness signatures when anisotropy values are used alongside bed-roughness measurements (Figs 9c and 10c, Table 2). Drumlin, megagroove and MSGL fields (areas 2, 3 and 4) show substantial anisotropy (≤ -0.2) compared to the cnoc and lochan (area 1) and mixed areas 5 and 6 (≥ -0.1). In most cases, anisotropy is negative, which is where bed roughness is higher orthogonal to palaeo-ice-flow direction (related to ice streamlining; Figs 9a and 10a). This type of anisotropy in essence describes elongation ratios of glacial landforms, which is thought

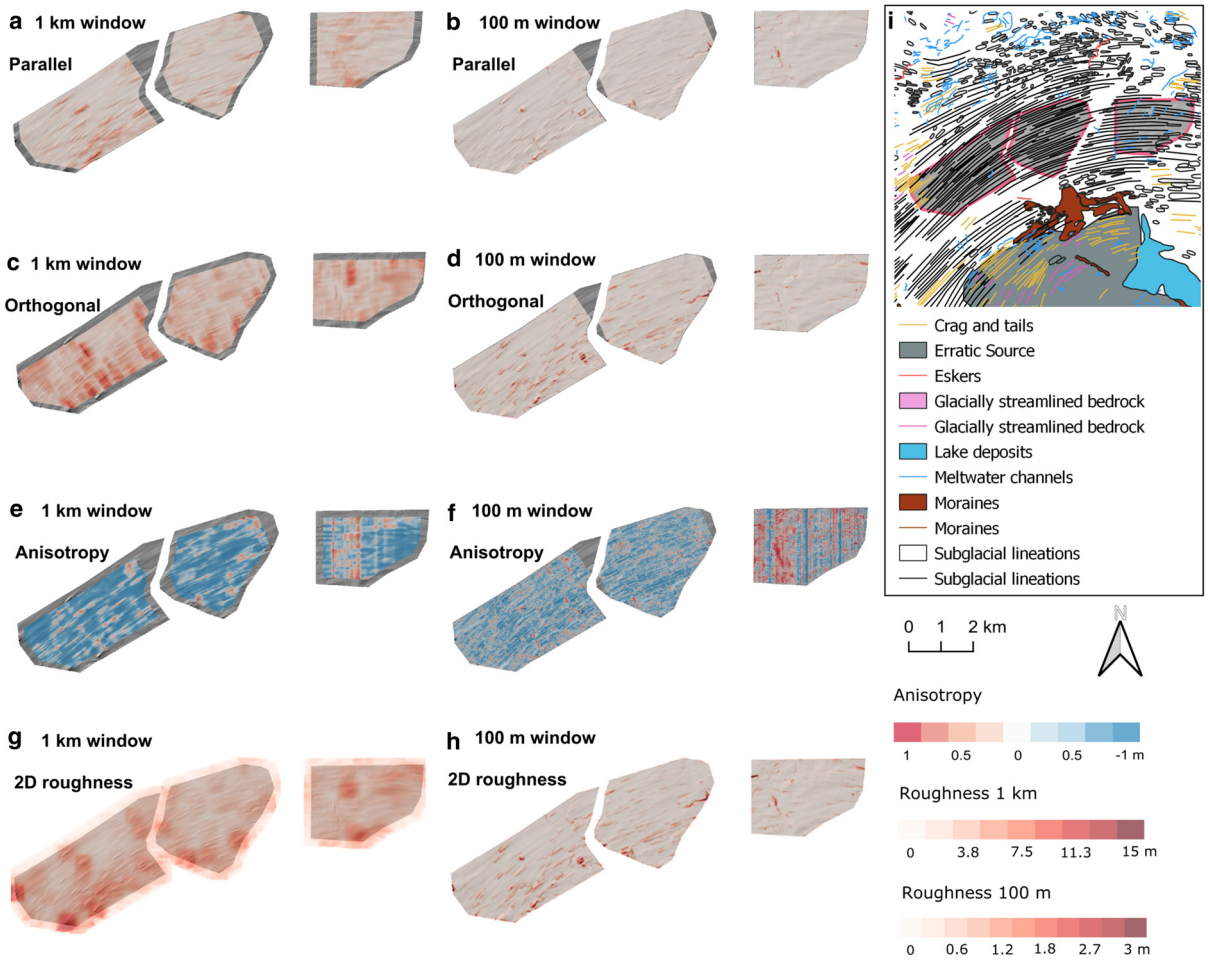

Fig. 7. Bed roughness over the Tyne Gap mixed lowlands (area 5). Bed roughness was calculated parallel (a, b) and orthogonal (c, d) to palaeo-ice flow direction (1-D), and for all flow directions (2-D; g, h), using SD with 1 km and 100 m window sizes. (e, f) Anisotropy of bed roughness was calculated at the crossover points between parallel and orthogonal transects for both window sizes. Between −1 and 0, orthogonal -roughness values dominate (blue). Between 0 and 1, parallel bed-roughness values dominate (red). At 0, bed roughness is isotropic (white). (i) Location area from Fig. 1 overlain with glacial landforms for comparison.

to directly relate to streamlining and ice velocity (Stokes and Clark, 1999; Spagnolo and others, 2017). The megagrooves and MSGLs (areas 3 and 4) have a higher mean anisotropy compared to the drumlins, which is consistent with the reported elongation values (6-25 : 1, 8-23 : 1, and 1-4 : 1 respectively; Mitchell, 1994; Everest and others, 2005; Bradwell and others, 2008). The areas that have mixed landforms are more isotropic, compared to the areas of uniform landforms (areas 2, 3 and 4) that have clear elongation ratios. Along with studies that demonstrate the effect of transect orientation on bed-roughness results (e.g. Gudlaugsson and others, 2013; Rippin and others, 2014; Bingham and others, 2015; Falcini and others, 2018; Cooper and others, 2019), these outcomes underline the importance of considering the anisotropy of bed roughness. Transects orientated parallel and orthogonal to ice flow are needed to calculate the anisotropy of bed roughness, and there are large datasets in Antarctica and Greenland that fit this criterion (e.g. Bingham and Siegert, 2009; King and others, 2009; Rippin, 2013; Lindbäck and Pettersson, 2015; Bingham and others, 2017).

Both the megagrooves (area 3) and the cnoc and lochan (area 1) are underlain by hard bedrock, with very little sediment cover (Bradwell, 2005; Bradwell and others, 2008; Krabbendam and Bradwell, 2014). Using the 1 km window size, both areas show similar mean bed roughness and anisotropy (Table 2 and Fig 9c). Yet, at smaller roughness scales (100 m window), the results show a clear difference between the cnoc and lochan (area 1) and megagrooves (area 3) (Figs 9c and 10c), with the megagrooves being considerably more anisotropic than the cnoc and lochan terrain. This difference in anisotropy between areas 1 and 3 is linked to the underlying geology. The fracture and joints of the basement gneiss in Assynt (area 1 location) are in essence isotropic whereas sedimentary and metasedimentary rocks often have highly anisotropic bedding planes (Krabbendam and Bradwell, 2014), which can be preferentially eroded to form megagrooves (Krabbendam and Glasser, 2011; Krabbendam and others, 2016).

The MSGLs (area 4) have a higher anisotropy for the 1 km window results compared to the 100 m window results. The MSGLs (area 4) are the only uniform landform area where this occurs (Figs 9a and 10a). The MSGLs typically have a spacing between landforms of 200–800 m and can be more than 200 m wide (Bradwell and others, 2008). Therefore, the bed-roughness signature is more distinct for the MSGLs (area 4) when using the 1 km window size because the 100 m window results may fall within the scale of an individual landform, and does not capture the roughness of the terrain as a whole.

The results indicate that a combination of bed roughness and bed-roughness anisotropy, can be used to differentiate uniform areas of landforms from each other, as well as from mixed areas of landforms. It should be noted that this is not 100% successful. The cnoc and lochan landscape (area 1) is the only uniform area that plots with the mixed landforms (at the 100 m window scale) due to the isotropic nature of the bed roughness here. There is also some crossover between other areas such as the drumlins

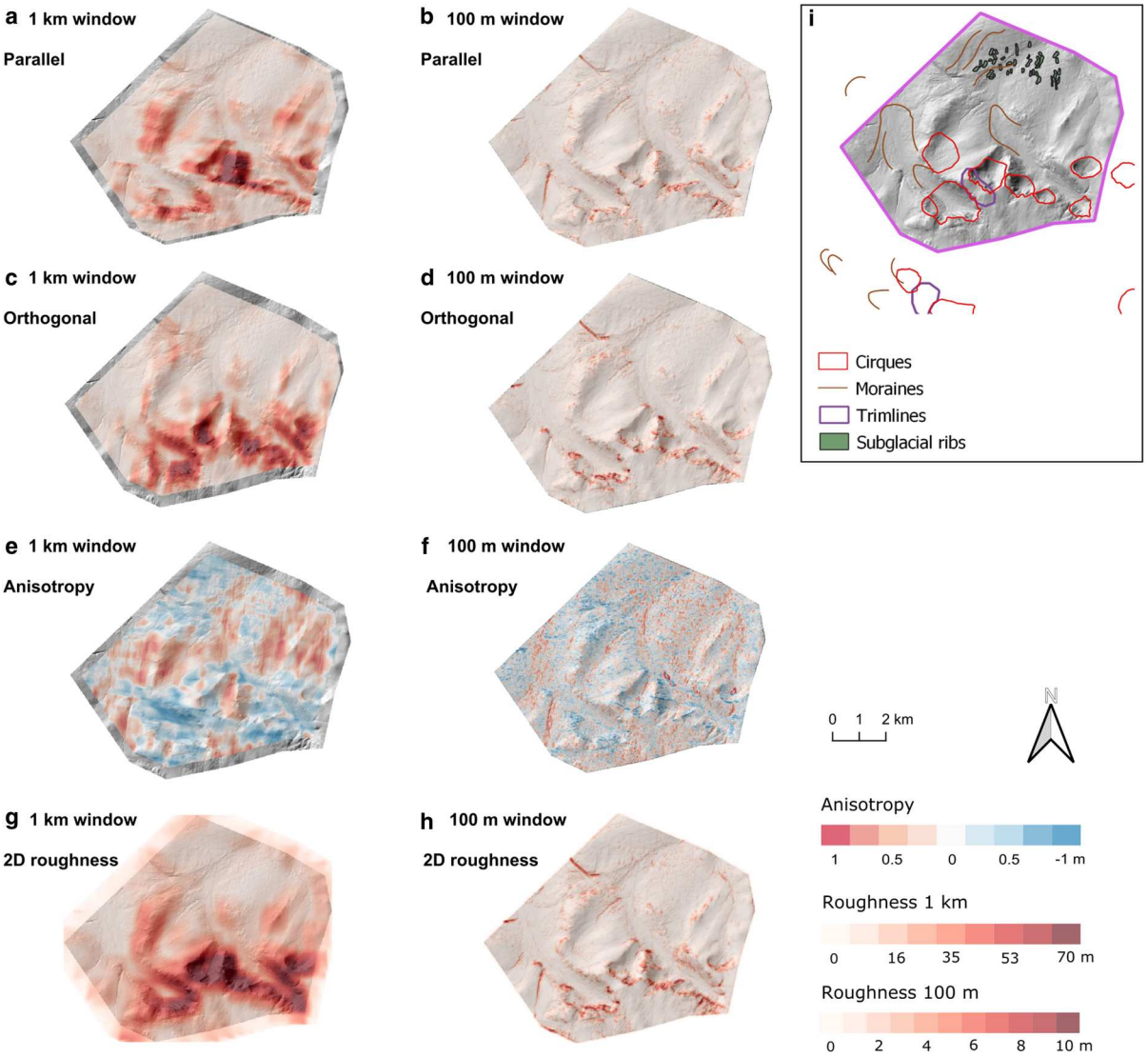

Fig. 8. Bed roughness over the Beinn Dearg mixed uplands (area 6). Bed roughness was calculated parallel (a, b) and orthogonal (c, d) to palaeo-ice flow direction (1-D), and for all flow directions (2-D; g, h), using SD with 1 km and 100 m window sizes. (e, f) Anisotropy of bed roughness was calculated at the crossover points between parallel and orthogonal transects for both window sizes. Between −1 and 0, orthogonal -roughness values dominate (blue). Between 0 and 1, parallel bed-roughness values dominate (red). At 0, bed roughness is isotropic (white). (i) Location area from Fig. 1 overlain with glacial landforms for comparison.

and megagrooves (areas 2 and 3; at the 100 m window scale) which is not surprising as some subglacial landforms are on a size-shape continuum (Ely and others, 2016).

Scale dependency

Due to the scale dependency of glacial landforms, the choice of window size has a significant impact on the bed-roughness results. Changing the window size will give different bed-roughness values for landforms because the window size sets the horizontal-scale range of the landforms being measured and it determines how much spatial averaging occurs (Smith, 2014). The mean bed-roughness values for all areas (except for the uplands, area 6; Table 2) show an order of magnitude difference in concert with the different window sizes. This means that bed-roughness measurements are only comparable between studies that use the same window size, as well as the same bed-roughness calculation (Falcini and others, 2018).

In most areas, the bed-roughness values derived using the 100 m window size identify individual glacial landforms more clearly than the 1 km window, even in the area of mixed glacial landforms, e.g. uplands (area 6). However, this is not the case for the MSGLs (area 4), demonstrating that one window size does not fit all glacial landforms. It is not just length and width of landforms that need to be taken into account but also spacing. For example, the megagrooves and MSGLs (areas 3 and 4) are similar landforms in terms of their shape. However, the megagrooves typically have a smaller spacing between landforms (100–500 m) compared to the MSGLs, and are narrower (50–150 m wide) (Bradwell and others, 2008). For anisotropic glacial landforms >100 m wide, the 100 m window size does not show the anisotropic nature as clearly as the 1 km window size. Thus, the 100 m window size may be more appropriate for mesoscale glacial landforms (1 m–1 km; Bennett and Glasser, 2009) such as drumlins, and some highly anisotropic macroscale landforms such as megagrooves, while the 1 km window size may be better suited to macroscale glacial landforms (1 km–100 km; Bennett and Glasser, 2009). Both window sizes are important for defining bed-roughness signatures.

Implications and applications

If bed-roughness signatures are consistent across uniform areas of glacial landforms, it will allow bed roughness from contemporary-ice streams to be used to infer the geomorphology that might

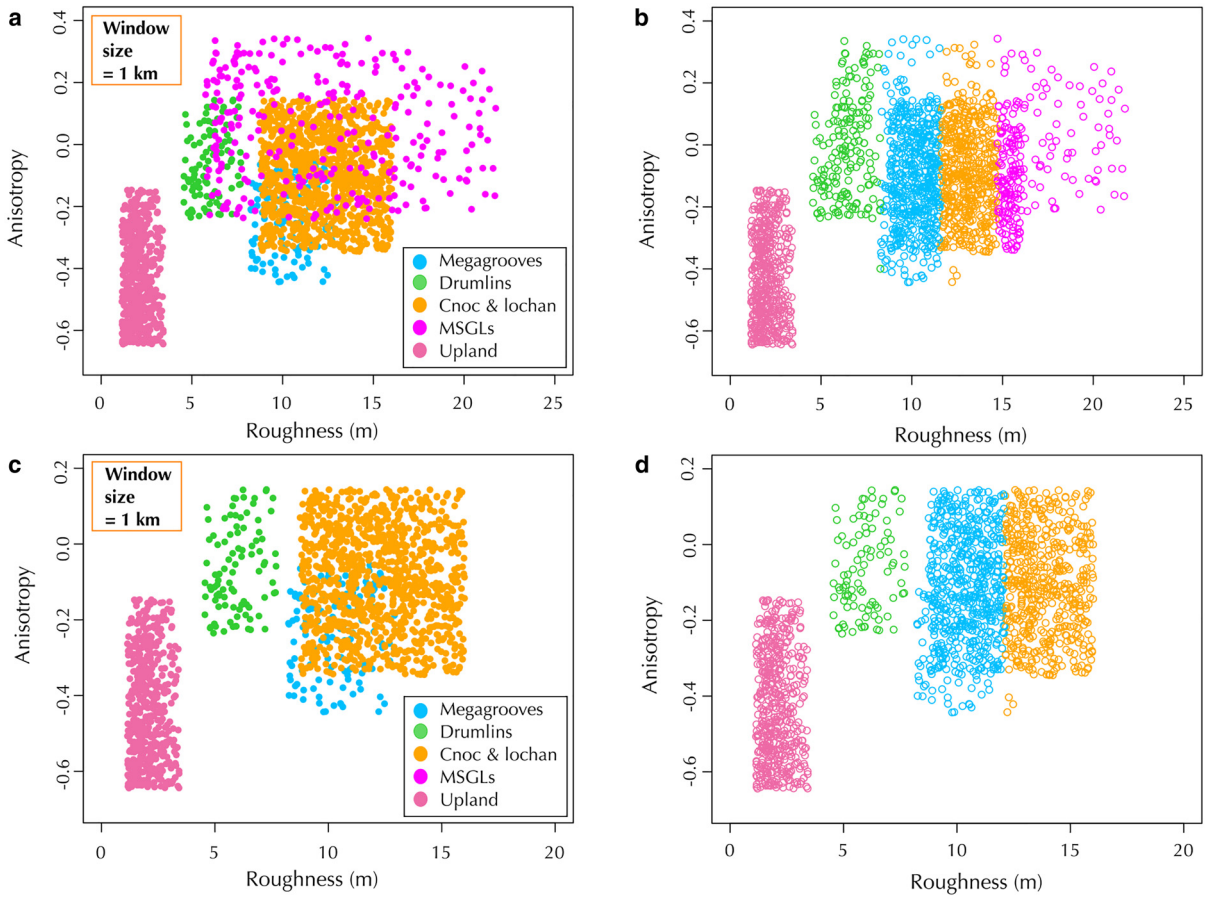

Fig. 9. Cluster analysis of bed roughness vs anisotropy for all areas except for area 5. (a) All the values derived using a 1 km window size colour coded by landform type (i.e. by area). (b) The results of cluster analysis. The cluster groups are colour coded to match the landform groups. The overall accuracy of the cluster analysis groups compared to the real landform groups was 58%. The accuracy for each area was 64% for area 1 (cnoc and lochan), 98% for area 2 (drumlins), 49% for area 3 (megagrooves), 100% for area 4 (MSGLs) and 62% for area 6 (Upland). (c) The same as (a) but only uniform landform sites were used (i.e. sites 1–4). (d) The same as (b) but only using the data from (c). The overall accuracy of the cluster analysis groups compared to the real landform groups was 71%. The accuracy for each area was 74% for area 1 (cnoc and lochan), 100% for area 2 (drumlins), 78% for area 3 (megagrooves) and 100% for area 4 (MSGLs).

exist at the bed (Schroeder and others, 2014; Stokes, 2018). This creates a new avenue of research to explore, and the potential to answer questions about ice-sheet beds. By using bed-roughness signatures to identify landform assemblages beneath contemporary-ice streams we could then be able to categorise them as either soft-bedded or hard-bedded (Stokes, 2018). The existing understanding of landform evolution is limited and there is no current consensus on certain landform formation mechanisms (e.g. drumlins and MSGLs; Clark, 2010; Spagnolo and others, 2014). If bed roughness can be used to infer where these landforms exist underneath contemporary-ice sheets, it will allow observations of how these landforms change over time in relation to ice dynamics, subglacial water routing, and address whether landforms are in a steady state (Schoof, 2002; Hillier and others, 2013; Stokes, 2018). Current observations mostly offer a single snapshot of the bed but a multi-temporal data acquisition strategy would be required to capture these processes. Furthermore, observations of landforms at the bed of contemporary-ice streams could be used to create statistical models that link subglacial processes to bedform metrics (Hillier and others, 2016). Finally, if areas of uniform landforms can be identified beneath contemporary-ice sheets, then the velocities associated with these areas can be used to refine velocities that are applied to model palaeo-ice sheets (e.g. Hubbard and others, 2009; Gandy and others, 2018).

This is the first study that has attempted to find bed-roughness signatures of uniform glacial landforms using 1-D methods. Repetition of this study at other areas, and other landform assemblages such as Rogen moraines, would be beneficial in order to constrain further the novel measurement of landform bed-roughness signatures. An important aspect of future research would be to test an area underneath a contemporary-ice sheet where uniform glacial landforms exist. This could, for example, be undertaken on the MSGLs underneath Rutford Ice Stream (King and others, 2007, 2009) or lineated bedforms underneath Pine Island Glacier (Bingham and others, 2017). Investigating whether landforms underneath contemporary-ice streams have similar bed roughness to those underneath palaeo-ice streams would allow a better understanding of basal conditions. We also show that bed roughness and anisotropy values for all areas investigated are similar at lower-resolution grids (Table 3). This suggests that the bed-roughness signatures reported from the 5 m × 5 m resolution grids could be compared with bed-roughness signatures calculated using lower-resolution RES data from contemporary-ice sheets. There will be complications with investigating the bed-roughness signatures of landforms underneath contemporary-ice sheets e.g. relict landforms in relation to modern ice-flow direction and cross-cutting landforms, and these need to be considered.

Conclusions

The groups of glacial landforms investigated here have a characteristic bed-roughness signature when bed-roughness anisotropy is taken into account. Anisotropy is key to defining the bed-roughness signatures of glacial landforms assemblages because

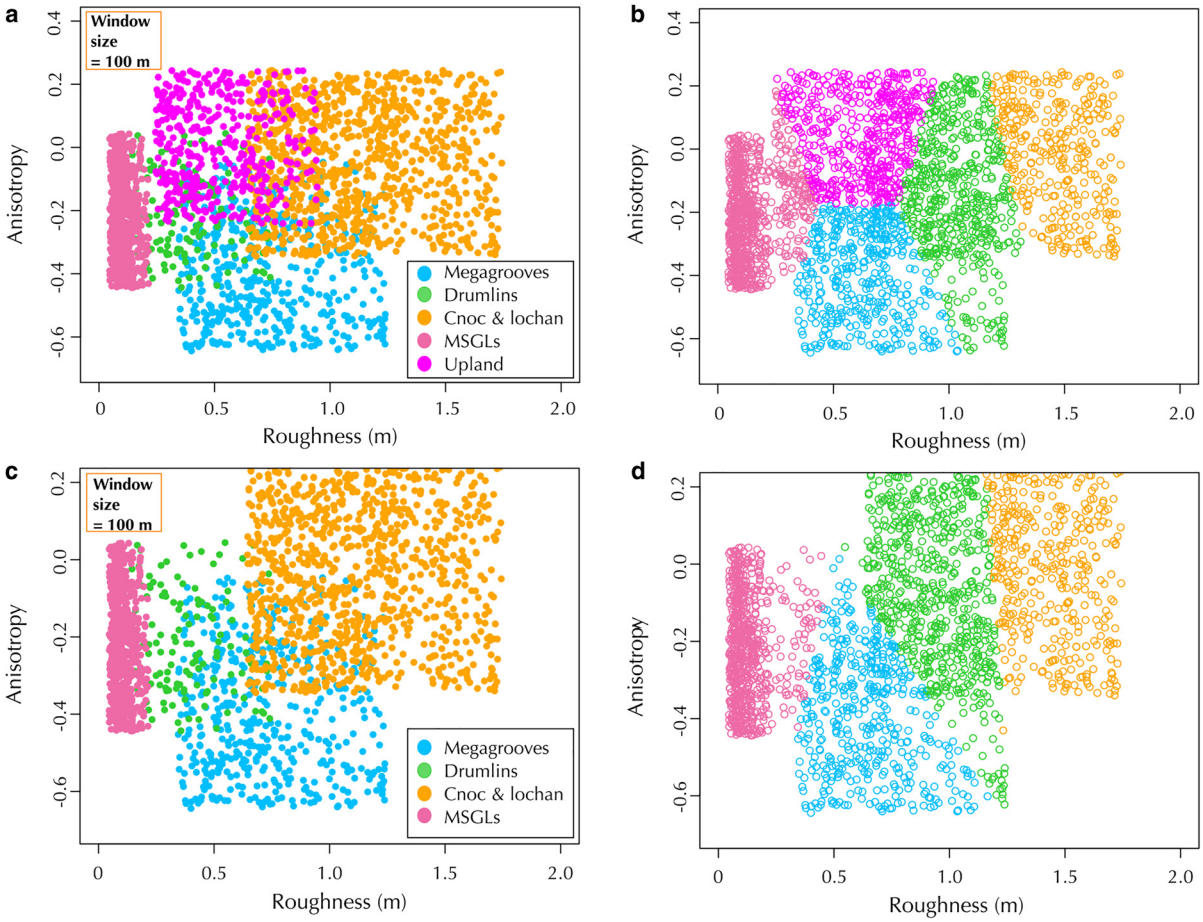

Fig. 10. Cluster analysis of bed roughness vs anisotropy for all areas except for area 5. (a) All the values derived using a 100 m window size colour coded by landform type (i.e. by area). (b) The results of cluster analysis. The cluster groups are colour coded to match the landform groups. The overall accuracy of the cluster analysis groups compared to the real landform groups was 60%. The accuracy for each area was 97% for area 1 (cnoc and lochan), 40% for area 2 (drumlins), 80% for area 3 (megagrooves), 96% for area 4 (MSGLs) and 77% for area 6 (Upland). (c) The same as (a) but only uniform landform sites were used (i.e. sites 1–4). (d) The same as (b) but only using the data from (c). The overall accuracy of the cluster analysis groups compared to the real landform groups was 65%. The accuracy for each area was 71% for area 1 (cnoc and lochan), 39% for area 2 (drumlins), 85% for area 3 (megagrooves) and 97% for area 4 (MSGLs).

Table 3. Mean values of bed roughness and anisotropy for all areas (m)

		Roughness mean			Anisotropy mean		
Area	Window size	1 km × 1 km	250 m × 250 m	5 m × 5 m	1 km × 1 km	250 m × 250 m	5 m × 5 m
1. Assynt cnoc and lochan	1 km	13.9	13	12.9	−0.1	−0.1	−0.1
	100 m	1	1.4	1.2	0	0	0
2. Ribblesdale drumlins	1 km	6.2	6.2	6.2	−0.1	−0.1	−0.1
	100 m	0.6	0.6	0.6	−0.3	−0.2	−0.2
3. Ullapool megagrooves	1 km	10.3	9.9	10.2	−0.2	−0.2	−0.2
	100 m	1	1	1	−0.4	−0.4	−0.3
4. Tweed MSGLs	1 km	2.5	2.5	2.5	−0.4	−0.4	−0.4
	100 m	0.2	0.2	0.2	−0.2	−0.2	−0.2
5. Tyne Gap lowlands	1 km	2.3	2.3	2.4	−0.2	−0.1	−0.1
	100 m	0.2	0.2	0.2	−0.1	0	0
6. Beinn Dearg uplands	1 km	15.3	16.8	16.6	0	0	0
	100 m	0.8	0.8	0.8	0	0	0

The means were calculated by combining values for both flow directions. In addition to the mean bed roughness and anisotropy for a 5 m × 5 m resolution grid reported in Table 2, we report values for 1 km × 1 km and 250 m × 250 m resolution grids.

this allows landforms with similar roughness values to be differentiated, e.g. cnoc and lochan and megagrooves (areas 1 and 3). This is the first study to show that glacial landforms have a characteristic bed-roughness signature, and this information could be used to infer the nature of landforms at the bed and where they are located underneath contemporary ice streams.

The results showed that a window size of 100 m was more appropriate for mesoscale and some macroscale landforms, whereas a window size of 1 km was better suited to macroscale landforms that were wider than 100 m and had a large spacing. However, both window sizes are required to determine the characteristic bed-roughness signatures of a wide range of landform types. It must be noted that to facilitate comparison between studies, window sizes must be the same. We suggest that this roughness-signature method needs to be further tested on other deglaciated areas before it can be used to identify landforms on contemporary-ice-sheet beds.

There are many unanswered questions about the environment at the bed of ice streams, such as how are landforms created, and

what processes are involved in their growth over time? How do changes in landform dimensions affect bed roughness, and consequently affect ice velocity? There are certain feedback loops that occur. The geomorphology of the bed influences ice velocity e.g. a rough bed causes slow speeds, but ice flow can smooth the shape of the bed and thus increase in speed. Finding out more information about this feedback loop is important because it could be key in our understanding of ice-stream beds. We have demonstrated that bed-roughness measurements with anisotropy data can be used to start to answer some of these questions.

Acknowledgements. This paper is dedicated to Nilo Falcini, who had a great scientific mind and a keen interest in understanding the Earth. Many thanks to Jon Hill and Colin McClean from the Environment and Geography Department at the University of York, who provided advice and guidance on the methods used. We thank the sub-editor and editor (Iestyn Barr and Hester Jiskoot) and two reviewers (Jeremy Ely and one anonymous reviewer) for their helpful and insightful comments, which significantly improved this paper. This research is part of a Ph.D. project, funded by NERC, grant number NE/K00987/1. OS Meridian data were provided by the Ordnance Survey, Crown copyright and database right 2012. NEXTMap DTM was provided by NERC via the Centre for Environmental Data Analysis (CEDA).

References

Benn DI and Evans DJA (2010) *Glaciers & Glaciation*, 2nd Edn. Abingdon: Hodder Education.

Bennett MR and Glasser NF (2009) *Glacial Geology*, 2nd Edn. Chichester: Wiley-Blackwell.

Bingham RG and 9 others (2015) Ice-flow structure and ice dynamic changes in the Weddell Sea sector of West Antarctica from radar-imaged internal layering. *Journal of Geophysical Research* **120**, 656–670. doi: 10.1002/2014JF003291.Received

Bingham RG and 12 others (2017) Diverse landscapes beneath Pine Island Glacier influence ice flow. *Nature Communications* **8**, 1618. doi: 10.1038/s41467-017-01597-y

Bingham RG and Siegert MJ (2009) Quantifying subglacial bed roughness in Antarctica: implications for ice-sheet dynamics and history. *Quaternary Science Reviews* **28**, 223–236. doi: 10.1016/j.quascirev.2008.10.014

Bingham RG, Siegert MJ, Young DA and Blankenship DD (2007) Organized flow from the South Pole to the Filchner-Ronne ice shelf: an assessment of balance velocities in interior East Antarctica using radio echo sounding data. *Journal of Geophysical Research* **112**, F03S26. doi: 10.1029/2006JF000556

Bradwell T (2005) Bedrock megagrooves in Assynt, NW Scotland. *Geomorphology* **65**, 195–204. doi: 10.1016/j.geomorph.2004.09.002

Bradwell T (2013) Identifying palaeo-ice-stream tributaries on hard beds: mapping glacial bedforms and erosion zones in NW Scotland. *Geomorphology* **201**, 397–414. doi: 10.1016/j.geomorph.2013.07.014

Bradwell T and Stoker MS (2015) Submarine sediment and landform record of a palaeo-ice stream within the British–Irish Ice Sheet. *Boreas* **44**, 255–276. doi: 10.1111/bor.12111

Bradwell T, Stoker M and Krabbendam M (2008) Megagrooves and streamlined bedrock in NW Scotland: the role of ice streams in landscape evolution. *Geomorphology* **97**, 135–156. doi: 10.1016/j.geomorph.2007.02.040

Chiverrell RC and Thomas GSP (2010) Extent and timing of the Last Glacial Maximum (LGM) in Britain and Ireland: a review. *Journal of Quaternary Science* **25**, 535–549. doi: 10.1002/jqs.1404

Clark CD (1993) Mega scale lineations and cross-cutting ice-flow landforms. *Earth Surface Processes and Landforms* **18**, 1–29. doi: 10.1002/esp.3290180102

Clark PU and 8 others (2009) The Last Glacial Maximum. *Science* **325**, 710–714. doi: 10.1126/science.1172873

Clark CD (2010) Emergent drumlins and their clones: from till dilatancy to flow instabilities. *Journal of Glaciology* **56**, 1011–1025. doi: 10.3189/002214311796406068

Clark CD and 13 others (2018a) BRITICE Glacial Map, version 2: a map and GIS database of glacial landforms of the last British–Irish Ice Sheet. *Boreas* **47**, 11–27. doi: 10.1111/bor.12273

Clark CD and 5 others (2018b) Spatial organization of drumlins. *Earth Surface Processes and Landforms* **43**(2), 499–513.

Clark CD, Hughes ALC, Greenwood SL, Jordan C and Sejrup HP (2012) Pattern and timing of retreat of the last British–Irish Ice Sheet. *Quaternary Science Reviews* **44**, 112–146. doi: 10.1016/j.quascirev.2010.07.019

Cooper MA, Jordan TM, Siegert MJ and Bamber JL (2019) Surface expression of basal and englacial features, properties, and processes of the Greenland ice sheet. *Geophysical Research Letters* **46**(2), 783–793. doi: 10.1029/2018GL080620

Crawley MJ (2007) *The R Book*, 1st Edn. Chichester: Wiley.

Davies BJ and 5 others (2019) Dynamic ice stream retreat in the central sector of the last British–Irish Ice Sheet. *Quaternary Science Reviews* **225**, 105989. doi: 10.1016/j.quascirev.2019.105989

Dowling TPF, Spagnolo M and Möller P (2015) Morphometry and core type of streamlined bedforms in southern Sweden from high resolution LiDAR. *Geomorphology* **236**, 4–63. doi: 10.1016/j.geomorph.2015.02.018

Ely JC and 7 others (2016) Do subglacial bedforms comprise a size and shape continuum?. *Geomorphology* **257**, 108–119. doi: 10.1016/j.geomorph.2016.01.001

Evans D, Archer S and Wilson DJH (1999) A comparison of the lichenometric and Schmidt hammer dating techniques based on data from the proglacial areas of some Icelandic glaciers. *Quaternary Science Reviews* **18**, 13–41. doi: 10.1016/S0277-3791(98)00098-5

Everest J, Bradwell T and Golledge N (2005) Subglacial landforms of the Tweed palaeo-ice stream. *Scottish Geographical Journal* **121**, 163–173. doi: 10.1080/00369220518737229

Falcini FA, Rippin DM, Krabbendam M and Selby KA (2018) Quantifying bed roughness beneath contemporary and palaeo-ice streams. *Journal of Glaciology* **64**, 822–834. doi: 10.1017/jog.2018.71

Finlayson A, Golledge N, Bradwell T and Fabel D (2011) Evolution of a Lateglacial mountain icecap in northern Scotland. *Boreas* **40**, 536–554. doi: 10.1111/j.1502-3885.2010.00202.x

Fretwell P and 44 others (2013) Bedmap2: improved ice bed, surface and thickness datasets for Antarctica. *The Cryosphere* **7**, 375–393. doi: 10.5194/tc-7-375-2013

Gandy N and 7 others (2018) Marine ice sheet instability and ice shelf buttressing influenced deglaciation of the Minch Ice Stream, Northwest Scotland. *The Cryosphere* **12**, 3635–3651. doi: 10.5194/tc-2018-116

Gudlaugsson E, Humbert A, Winsborrow M and Andreassen K (2013) Subglacial roughness of the former Barents Sea ice sheet. *Journal of Geophysical Research* **118**, 2546–2556. doi: 10.1002/2013JF002714

Hartigan JA and Wong MA (1979) Algorithm as 136: a *k*-means clustering algorithm. *Journal of the Royal Statistical Society. Series C (Applied Statistics)* **28**(1), 100–108.

Hillier JK and 5 others (2016) Exploring explanations of subglacial bedform sizes using statistical models. *PLoS One* **11**, 1–29. doi: 10.1371/journal.pone.0159489

Hillier JK, Smith MJ, Clark CD, Stokes CR and Spagnolo M (2013) Subglacial bedforms reveal an exponential size-frequency distribution. *Geomorphology* **190**, 82–910. doi: 10.1016/j.geomorph.2013.02.017

Holschuh N, Christianson K, Paden J, Alley R and Anandakrishnan S (2020) Linking postglacial landscapes to glacier dynamics using swath radar at Thwaites Glacier, Antarctica. *Geology* **48**(3), 268–272. doi: 10.1130/G46772.1

Hubbard A and 7 others (2009) Dynamic cycles, ice streams and their impact on the extent, chronology and deglaciation of the British–Irish ice sheet. *Quaternary Science Reviews* **28**, 758–776. doi: 10.1016/j.quascirev.2008.12.026

Hughes ALC, Clark CD and Jordan CJ (2010) Subglacial bedforms of the last British Ice Sheet. *Journal of Maps* **6**, 543–563. doi: 10.4113/jom.2010.1111

Hughes ALC, Clark CD and Jordan CJ (2014) Flow-pattern evolution of the last British Ice Sheet. *Quaternary Science Reviews* **89**, 148–168. doi: 10.1016/j.quascirev.2014.02.002

Intermap Technologies (2009) NEXTMap British Orthorectified Radar Image (ORI) Data by Intermap.

Jezek K and 6 others (2011) Radar images of the bed of the Greenland Ice Sheet. *Geophysical Research Letters* **38**, L01501. doi: 10.1029/2010GL045519

King EC, Hindmarsh RCA and Stokes CR (2009) Formation of mega-scale glacial lineations observed beneath a West Antarctic ice stream. *Nature Geoscience* **2**, 585–588. doi: 10.1038/ngeo581

King EC, Pritchard HD and Smith AM (2016) Subglacial landforms beneath Rutford Ice Stream, Antarctica: detailed bed topography from ice-penetrating radar. *Earth System Science Data* **8**, 151–158. doi: 10.5194/essd-8-151-2016

King EC, Woodward J and Smith AM (2007) Seismic and radar observations of subglacial bed forms beneath the onset zone of Rutford Ice Stream, Antarctica. *Journal of Glaciology* **53**, 665–672. doi: 10.3189/002214307784409216

Kleman J, Hättestrand C, Borgström I and Stroeven A (1997) Fennoscandian palaeoglaciology using a glacial geological inversion model. *Journal of Glaciology* **43**, 283–299.

Krabbendam M and Bradwell T (2014) Quaternary evolution of glaciated gneiss terrains: pre-glacial weathering vs glacial erosion. *Quaternary Science Reviews* **95**, 20–42. doi: 10.1016/j.quascirev.2014.03.013

Krabbendam M, Eyles N, Putkinen N, Bradwell T and Arbelaez-Moreno L (2016) Streamlined hard beds formed by palaeo-ice streams: a review. *Sedimentary Geology* **338**, 24–50. doi: 10.1016/j.sedgeo.2015.12.007

Krabbendam M and Glasser NF (2011) Glacial erosion and bedrock properties in NW Scotland: abrasion and plucking, hardness and joint spacing. *Geomorphology* **130**, 374–383. doi: 10.1016/j.geomorph.2011.04.022

Kulessa B and 10 others (2017) Seismic evidence for complex sedimentary control of Greenland Ice Sheet flow. *Science Advances* **3**(8), 1–9. doi: 10.1126/sciadv.1603071

Leong WJ and Horgan HJ (2020) DeepBedMap: using a deep neural network to better resolve the bed topography of Antarctica. *The Cryosphere* **14**, 3687–3705. doi: 10.5194/tc-14-3687-2020

Li X and 7 others (2010) Characterization of subglacial landscapes by a two-parameter roughness index. *Journal of Glaciology* **56**, 831–836. doi: 10.3189/002214310794457326

Lindbäck K and Pettersson R (2015) Spectral roughness and glacial erosion of a land-terminating section of the Greenland ice sheet. *Geomorphology* **238**, 149–159. doi: 10.1016/j.geomorph.2015.02.027

Livingstone SJ and 8 others (2012) Glaciodynamics of the central sector of the last British–Irish Ice Sheet in Northern England. *Earth-Science Reviews* **111**, 25–55. doi: 10.1016/j.earscirev.2011.12.006

Livingstone SJ and 5 others (2015) Late Devensian deglaciation of the Tyne Gap Palaeo-Ice Stream, northern England. *Journal of Quaternary Science* **30**, 790–804. doi: 10.1002/jqs.2813

Livingstone SJ, Ó Cofaigh C and Evans DJ (2008) Glacial geomorphology of the central sector of the last British–Irish Ice sheet. *Journal of Maps* **4**, 358–377. doi: 10.4113/jom.2008.1032

Livingstone SJ, Ó Cofaigh C and Evans DJA (2010) A major ice drainage pathway of the last British–Irish Ice Sheet: the Tyne Gap, northern England. *Journal of Quaternary Science* **25**, 354–370. doi: 10.1002/jqs

MacGregor JA and 11 others (2016) A synthesis of the basal thermal state of the Greenland ice sheet. *Journal of Geophysical Research: Earth Surface* **121**, 1328–1350. doi: 10.1002/2015JF003803.Received

Margold M, Stokes CR and Clark CD (2015) Ice streams in the Laurentide Ice Sheet: identification, characteristics and comparison to modern ice sheets. *Earth-Science Reviews* **143**, 117–146. doi: 10.1016/j.earscirev.2015.01.011

Menzies J (1979) A review of the literature on the formation and location of drumlins. *Journal of Glaciology* **22**(87), 373–384.

Mercer B (2007) National and regional scale DEMs created from airborne INSAR. *Proceedings of PIA07 – Photogrammetric Image Analysis* **36**, 113–118.

Mitchell WA (1994) Drumlins in ice sheet reconstructions, with reference to the western Pennines, northern England. *Sedimentary Geology* **91**, 313–332.

Newton M, Evans DJA, Roberts DH and Stokes CR (2018) Bedrock mega-grooves in glaciated terrain: a review. *Earth-Science Reviews* **185**, 57–79. doi: 10.1016/j.earscirev.2018.03.007

Nias IJ, Cornford SL and Payne AJ (2016) Contrasting the modelled sensitivity of the Amundsen Sea Embayment ice streams. *Journal of Glaciology* **62**, 552–562. doi: 10.1017/jog.2016.40

Peck V and 6 others (2006) High resolution evidence for linkages between NW European ice sheet instability and Atlantic Meridional overturning circulation. *Earth and Planetary Science Letters* **243**(3), 476–488. doi: 10.1016/j.epsl.2005.12.023

Prescott PW (2013) Quantifying Subglacial Roughness and Its Link to Glacial Geomorphology and Ice Speed (Ph.D. thesis). Durham University, Durham, UK.

Rea BR and Evans DJA (1996) Landscapes of areal scouring in N.W. Scotland. *Scottish Geographical Magazine* **112**, 47–50. doi: 10.1080/00369229618736977

Rippin DM (2013) Bed roughness beneath the Greenland ice sheet. *Journal of Glaciology* **59**, 724–732. doi: 10.3189/2013JoG12J212

Rippin DM and 9 others (2014) Basal roughness of the Institute and Möller Ice Streams, West Antarctica: process determination and landscape interpretation. *Geomorphology* **214**, 139–147. doi: 10.1016/j.geomorph.2014.01.021

Rippin DM, Bamber JL, Siegert MJ, Vaughan DG and Corr HFJ (2006) Basal conditions beneath enhanced-flow tributaries of Slessor Glacier, East Antarctica. *Journal of Glaciology* **52**, 481–490. doi: 10.3189/172756506781828467

Schoof C (2002) Basal perturbations under ice streams: form drag and surface expression. *Journal of Glaciology* **48**(162), 407–416. doi: 10.3189/172756502781831269

Schroeder DM, Blankenship DD, Young DA, Witus AE and Anderson JB (2014) Airborne radar sounding evidence for deformable sediments and outcropping bedrock beneath Thwaites Glacier, West Antarctica. *Geophysical Research Letters* **41**, 7200–7208. doi: 10.1002/2014GL061645.Received

Shepard MK and 5 others (2001) The roughness of natural terrain: a planetary and remote sensing perspective. *Journal of Geophysical Research* **106**, 32777–32795.

Shepard MK and Campbell BA (1999) Radar scattering from a self-affine fractal surface: near-nadir regime. *Icarus* **141**, 156–171. doi: 10.1006/icar.1999.6141

Siegert MJ, Taylor J and Payne AJ (2005) Spectral roughness of subglacial topography and implications for former ice-sheet dynamics in East Antarctica. *Global and Planetary Change* **45**, 249–263. doi: 10.1016/j.gloplacha.2004.09.008

Siegert MJ, Taylor J, Payne AJ and Hubbard B (2004) Macro-scale bed roughness of the Siple Coast ice streams in west Antarctica. *Earth Surface Processes and Landforms* **29**, 1591–1596. doi: 10.1002/esp.1100

Smith MW (2014) Roughness in the earth sciences. *Earth-Science Reviews* **136**, 202–225. doi: 10.1016/j.earscirev.2014.05.016

Smith BE, Raymond CF and Scambos T (2006) Anisotropic texture of ice sheet surfaces. *Journal of Geophysical Research* **111**, 1–8. doi: 10.1029/2005JF000393

Sofia G, Pirotti F and Tarolli P (2013) Variations in multiscale curvature distribution and signatures of LiDAR DTM errors. *Earth Surface Processes and Landforms* **38**, 1116–1134. doi: 10.1002/esp.3363

Spagnolo M and 7 others (2014) Size, shape and spatial arrangement of mega-scale glacial lineations from a large and diverse dataset. *Earth Surface Processes and Landforms* **39**, 1432–1448. doi: 10.1002/esp.3532

Spagnolo M and 12 others (2017) The periodic topography of ice stream beds: insights from the Fourier spectra of mega-scale glacial lineations. *Journal of Geophysical Research* **122**, 1355–1373. doi: 10.1002/2016JF004154

Spagnolo M, Clark CD and Hughes ALC (2012) Drumlin relief. *Geomorphology* **153-154**, 179–191. doi: 10.1016/j.geomorph.2012.02.023

Stokes CR (2018) Geomorphology under ice streams: moving from form to process. *Earth Surface Processes and Landforms* **43**, 85–123. doi: 10.1002/esp.4259

Stokes CR and Clark CD (1999) Geomorphological criteria for identifying Pleistocene ice streams. *Annals of Glaciology* **28**, 67–74. doi: 10.3189/172756499781821625

Stokes CR and Clark CD (2001) Palaeo-ice streams. *Quaternary Science Reviews* **20**, 1437–1457. doi: 10.1016/S0277-3791(01)00003-8

Taylor J, Siegert MJ, Payne AJ and Hubbard B (2004) Regional-scale bed roughness beneath ice masses: measurement and analysis. *Computers and Geosciences* **30**, 899–908. doi: 10.1016/j.cageo.2004.06.007

Trevisani S and Cavalli M (2016) Topography-based flow-directional roughness: potential and challenges. *Earth Surface Dynamics* **4**(2), 343–358. doi: 10.5194/esurf-4-343-2016